Consequences of kinetic non-equilibrium for the nuclear equation-of-state in heavy ion collision

C. Fuchs[1] and T. Gaitanos[2]

[1] *Institut für Theoretische Physik der Universität Tübingen, Auf der Morgenstelle 14, D-72076 Tübingen, Germany*

[2] *Sektion Physik der Universität München, Am Coulombwall 1, D-85748 Garching, Germany*

Highly compressed nuclear matter created in relativistic heavy collisions is to large extent governed by local non-equilibrium. As an idealized scenario colliding nuclear matter configurations are studied within both, relativistic mean field theory and using more realistic in-medium interactions based on the Dirac-Brueckner T-matrix. The equation of state in anisotropic matter is thereby governed by two competing effects: The enlarged phase space volume in colliding matter tends to soften the internal potential energy of the subsystems whereas the relative motion of the two currents leads to a strong additional repulsion in the system. An effective EOS constructed for anisotropic momentum configurations shows a significant net softening compared to ground state nuclear matter. This effect is found to be to large extend independent on the particular choice of the nuclear interaction. A critical discussion of standard transport approaches with respect to the considered non-equilibrium effects is given.

I. INTRODUCTION

One major goal of relativistic heavy ion physics is to explore the behavior of the nuclear equation-of-state (EOS) far away from saturation, i.e. at high densities and non-zero temperature. Over the last three decades a large variety of observables has been investigated both, from the experimental and theoretical side motivated by the search for the nuclear

EOS. The collective particle flow is thereby intimately connected to the dynamics during the compressed high density phase of such reactions [1,2]. E.g., the elliptic flow which develops in the early compression phase is thought to be a suitable observable to extract information on the EOS [3]. But also the production of strange particles is a good probe to study dense matter [4]. Recent precision measurements of the K^+ production at SIS energies strongly support the scenario of a soft EOS [5,6].

However, the difficulty to extract information on the EOS $\epsilon(\varrho)$ from heavy ion reactions lies in the fact that the system is out of equilibrium. At intermediate energies the relaxation time needed to equilibrate coincides more or less with the high density phase of the reaction. Hence, non-equilibrium effects are present over the compression phase where one essentially intends to study the EOS at supra-normal densities. Experimental evidence for incomplete equilibration even in central collisions has recently been reported in [7]. In the early stages of the reaction, the phase space distribution in the participant zone is similar to two fluids of counter-streaming matter. The local momentum distributions of such colliding nuclear matter, called CNM in the following, are given by two Fermi ellipsoids, i.e. two boosted Fermi spheres separated by a relative velocity [8]. In the course of the reaction the mid-rapidity region is more and more populated due to binary collisions and the system is heated up. The originally cold and sharp momentum ellipsoids become diffuse and merge together. The energy density depends in the course of the reaction therefore on both, the *local* relative velocity and the *local* temperature:

$$\epsilon(\varrho, v_{\rm rel}, T=0) \longrightarrow \epsilon(\varrho, v_{\rm rel}, T) \longrightarrow \epsilon(\varrho, v_{\rm rel}=0, T) \quad .$$

In order to learn something about the ground state EOS one has to seperate the compression energy from the contributions of the relative motion and the thermal energy

$$\epsilon(\varrho, v_{\rm rel}, T) = \epsilon_{\rm comp} + \mathcal{E}_{\rm rel} + \mathcal{E}_{\rm therm}$$

This is generally a difficult task since the various contributions are not independent from each other. Moreover, the conversion of kinetic energy into compression and thermal energy

goes along with the production of entropy. While the total energy is conserved, the free energy tends to minimize. This temporal evolution of a heavy ion reaction is described by microscopic transport models like BUU [9] or QMD [10]. Such simulations [11–13] show also that the local phase space in the overlapping overlapping zone of two interpenetrating nuclei can to large extent be idealized by colliding nuclear matter. CNM provides a smooth transition to a final, at least in the central cell, fully equilibrated spherical momentum configuration.

The aim of the present work is to investigate in more detail how the compression energy, related to the *ground state* EOS, can be extracted in kinetic non-equilibrium situations and which consequences arise if one tries to do this by the use of dynamical transport simulations. In the limit of vanishing temperature the compression energy is just the free energy of the system $\epsilon_{\rm comp} = \epsilon(\varrho, v_{\rm rel}, T = 0) - \mathcal{E}_{\rm rel}$. To obtain an effective EOS in CNM one has to subtract the energy of the relative motion. Such a treatment neglects temperature effects but it allows to study non-equilibrium features for simplified configurations. These reflect in first order the phase space evolution in the initial and the high density phase of the reaction where termperatures are still moderate. Therefore the infinite counter-streaming two-fluid scenario has been a subject of a variety of theoretical investigations [8,14–20].

In transport calculations the nuclear mean field is usually based on phenomenological parameterizations [9,10,21,22]. Such parameterizations allow different extrapolations to high densities, summarized by referring to a 'hard' or a 'soft' equation-of-state [1], which can be tested in heavy ion collisions. A more microscopic approach is to start from free NN interactions, determine the correlated two-body interaction in nuclear matter and use this interaction in heavy ion reactions. Doing so, in each time step in the course of the reaction the mean field, respectively the EOS, would have to be derived from an integration of the two-body interaction over the actual momentum distribution. This determines then both, the density and the momentum dependence of the mean field [8,23–25]. In phenomenological approaches, even when momentum dependent interactions are included, part of the arising non-equilibrium features is missing. Also with phenomenological two-body interactions the

complete single particle potential should consistently be derived for the actual momentum configuration. In standard transport calculation this is, however, not done: the single particle potential contains a purely density dependent part which, as a density functional, has been determined for equilibrium matter. The momentum dependent part, on the other hand, accounts in lowest order for anisotropy and temperature effects of the phase space distribution. However, the density dependent part is that one which is most directly related to the ground state EOS.

To obtain a model independent picture the present investigations are based on different choices of the nuclear forces. We use the framework of relativistic mean field theory, i.e. the Walecka model [26,27] and the microscopic relativistic Dirac-Brueckner (DB) approach [28,29]. The mean field approach has the advantage that most integrals can be evaluated analytically which makes the discussion of typical features of CNM more transparent. The DB model, on the other side, is more realistic. It turned out to be quite successful in the description of nuclear matter bulk properties. DB forces have been extensively tested at SIS energies below 1 A.GeV, and a general agreement with corresponding flow data has been observed [22,25,30]. Other studies of CNM have been performed in a non-relativistic framework using either Skyrme interactions [16,13] or Brueckner G-matrix forces [14,18]. Relativistically colliding matter has been mainly treated within the Walecka model [8,15,17,19]. In [8] a first attempt was made to apply relativistic DB forces. In some cases also finite temperature effects have been studied [20,19]. In [13] T dependent G-matrix forces were used in transport simulations but the influence of the explicit T dependence of the mean field on the reaction dynamics was found to be moderate.

The paper is organized as follows: In Sec.2 we discuss the general structure of the relativistic energy-momentum tensor in colliding nuclear matter within both, the DB and the mean field (MF) approach. In Sec.3 we derive an effective EOS for the CNM configuration. In Sec.4 implications for heavy ion reactions are discussed, in particular with respect to transport calculations. In Sec.5 we give some short remarks concerning the treatment in non-relativistic approaches and finally conclude in Sec.6.

II. ENERGY-MOMENTUM TENSOR IN COLLIDING NUCLEAR MATTER

The phase space distribution of colliding nuclear matter (CNM)

$$\Theta_{12} = \Theta_1 + \Theta_2 - \Theta_1 \cdot \Theta_2 \tag{1}$$

is composed by the momentum distributions of two counter-streaming matters $\Theta_i = \Theta(\mu^*(k_{F_i}) - k^*_\nu u^\nu_i)$, i.e. two boosted Fermi ellipsoids. Θ is the step function, k_{F_i} are the Fermi momenta and $u^\nu_i = (\gamma_i, \gamma_i \mathbf{u}_i)$ are the streaming velocities of the two subsystem currents. The last term in eq. (1) ensures that the Pauli principle is fulfilled for small velocities where the two ellipsoids might overlap. The total baryon density has thereby to be restored. Details of this procedure which can be performed by a covariant construction can be found in [8].

A. DB approximation

The interaction of nucleons with the surrounding medium is expressed in terms of a self energy which dresses the particles, respectively the in-medium propagator. Analogous to spin-isospin saturated nuclear matter at rest, the self energy in colliding matter can be decomposed into scalar and vector components expressed covariantly by

$$\Sigma(k) = \Sigma_S(k) - \gamma_\mu \Sigma^\mu(k) \tag{2}$$

$$\Sigma_\mu(k) = \Sigma_0(k) u_{\mu 12} + \Sigma_v(k) \Delta^{\mu\nu}_{12} k_\nu \quad . \tag{3}$$

Here, the Σ_i with $i = S, 0, v$ are scalar functions.

The four–velocity u^μ_{12} is the streaming velocity of the combined system derived from the total current $j^\mu_{12} = \varrho_{12} u^\mu_{12}$. Since ϱ_{12} is the invariant baryon density in the c.m. frame of the two currents, $\varrho_{12} = \sqrt{j^2_{12}} =< 1 >_{12} |_{c.m.}$, it is natural to work in that frame, i.e. the frame where the sum of the spatial components of the two counter-streaming currents vanish $\mathbf{j}_{12} = 0$. With the help of the projector perpendicular to u^μ_{12}

$$\Delta^{\mu\nu}_{12} = g^{\mu\nu} - u^\mu_{12} u^\nu_{12} \tag{4}$$

eqs. (3) are manifestly covariant. Inversely, the self-energy components are obtained from covariant projections

$$\Sigma_S = \frac{1}{4}\mathrm{tr}[\Sigma] \tag{5}$$

$$\Sigma_0 = \frac{-1}{4}\mathrm{tr}\left[u_{12}^{\mu}\gamma_{\mu}\Sigma\right] \tag{6}$$

$$\Sigma_v = \frac{-1}{4\left(\Delta_{12}^{\mu\nu}k_{\mu}k_{\nu}\right)}\mathrm{tr}\left[\Delta_{12}^{\mu\nu}k_{\mu}\gamma_{\nu}\Sigma\right] \quad . \tag{7}$$

One should note that in this form the projections are identical to nuclear matter at rest [28] except for the fact that all quantities are determined in the colliding system. Hence the effective mass and the kinetic momenta are given by

$$M^* = M + \Sigma_S(k) \tag{8}$$

$$k_{\mu}^* = k_{\mu} + \Sigma_{\mu}(k) \tag{9}$$

$$E^* = \sqrt{\mathbf{k}^{*2} + M^{*2}(k)} \quad . \tag{10}$$

The self-energy has now to be derived from some model, e.g. from an effective two-body interaction like the in-medium T-matrix. In this general case the self-energy components (3-10) are momentum dependent. We also consider the mean field approach of the Walecka model [26] where the self-energies are not explicitely momentum dependent. This has the advantage that all integrals can be solved analytically. In the DB approach it is useful to introduce an additional configuration averaged and momentum independent effective mass. In the c.m. frame ($\mathbf{j}_{12} = 0$) one can thus get rid of the Σ_v contribution by rescaling the fields in the same way as it is done in nuclear matter [28,29]. The spatial component of the self-energy (7) has in the c.m. frame the form $\mathbf{\Sigma} = \Sigma_v(k)\mathbf{k}$. In NM Σ_v has been found to be small and nearly constant as a function of momentum. In mean field theory this contribution vanishes identically. Here it can be absorbed into a rescaled effective mass

$$\tilde{M}^* = \frac{M + \overline{\Sigma}_S}{1 + \overline{\Sigma}_v} \tag{11}$$

and the rescaled momentum $\tilde{\mathbf{k}}^* = \mathbf{k}^*/(1 + \overline{\Sigma}_v) = \mathbf{k}|_{c.m.}$. The configuration-averaged scalar and vector self-energy components are defined as

$$\overline{\Sigma}_S = < \Sigma_S(k)\tilde{M}^*/\tilde{E}^* >_{12} /\varrho_{S_{12}} \tag{12}$$

$$\overline{\Sigma}_v = < \Sigma_v(k)/\tilde{E}^* >_{12} / < 1/\tilde{E}^* >_{12} \quad . \tag{13}$$

Here

$$< X >_{12} = \frac{\kappa}{(2\pi)^3} \int d^3\mathbf{k} X(k) \Theta_{12}(k;\chi) \tag{14}$$

denotes the summation over all occupied states and $\tilde{E}^*$ is defined as in (10), however, with the rescaled quantities $\tilde{M}^*$ and $\tilde{\mathbf{k}}^*$. In spin-isospin saturated nuclear matter the phase space occupancy factor in (14) equals $\kappa = 4$. The set of parameters which determines the colliding configuration is denoted by $\chi = \{k_{F_1}, k_{F_2}, u_1, u_2, \tilde{M}^*\}$. Thus the effective mass $\tilde{M}^*$, the scalar density $\varrho_{S_{12}} =< \tilde{M}^*/\tilde{E}^* >_{12}$ and the configuration (1) itself are coupled by non-linear equations. The Dirac part of the in-medium propagator has the same form as in nuclear matter [26,31]

$$G_{12}(k) = [\gamma_\mu \tilde{k}^{*\mu} + \tilde{M}^*] 2\pi i \delta(\tilde{k}^{*2} - \tilde{M}^{*2}) 2\Theta(\tilde{k}_0^*) \Theta_{12}(k;\chi) \quad . \tag{15}$$

It should be noticed that the usage of an averaged effective mass in the propagator is a standard procedure of the DB approach [28,29] (reference spectrum approximation). It is based on the observation that M^* is only weakly varying with momentum inside the Fermi sea and it simplifies the solution of the Bethe-Salpeter equation considerably. To account for the full momentum dependence of the effective mass in the two-body propagator of the BS-equation is presently beyond the scope of DB calculations. In CNM this approximation is more severe due to large relative momenta which can occur between the two currents. However, since the effective mass shows in DB calculations only a rather moderate momentum dependence at large momenta above the Fermi surface [29] this approximation is still justified. The self-energy components follow now from covariant projections of the T-matrix elements. For on-shell scattering of positive energy states the T-matrix can generally be decomposed into five Lorentz invariant amplitudes (scalar, vector, tensor, axial vector and pseudo-scalar or pseudo-vector, respectively) [31,28] where direct (Hartree) and exchange

(Fock) amplitudes are related by a Fierz transformation [32]. If the amplitudes are already anti-symmetrized the 'direct' representation for the T-matrix is sufficient [29]

$$\begin{aligned}\Sigma(k) &= -i\int \frac{d^4q}{(2\pi)^4}\mathrm{tr}\left[G_{12}(q)\ T(k,q;\chi)\right] \\ &= \frac{\kappa}{(2\pi)^3}\int \frac{d^3\mathbf{q}}{\tilde{E}^*(\mathbf{q})}\left[\tilde{M}^* T_{\mathrm{S}}(k,q;\chi) + \not{q}^* T_{\mathrm{V}}(k,q;\chi)\right]\Theta_{12}(q;\chi)\quad . \end{aligned} \tag{16}$$

The scalar T_{S} and the vector T_{V} amplitude are Lorentz invariant functions which depend (besides the parametric dependence on the configuration expressed by χ) on the c.m. momentum, the c.m. relative momentum and the c.m. scattering angle between k and q in a Lorentz invariant manner which can be converted to a dependence on the Mandelstam variables s^*, t^*, u^*.

The energy momentum tensor in CNM is given by

$$\begin{aligned}T^{\mu\nu} &= -i\int \frac{d^4k}{(2\pi)^4}\mathrm{tr}\left[\gamma^\mu G_{12}(k)\right]k^\nu - \frac{i^2}{2}g^{\mu\nu}\int \frac{d^4k}{(2\pi)^4}\frac{d^4q}{(2\pi)^4}\mathrm{tr}\left[G_{12}(k)\ \mathrm{tr}\left[G_{12}(q)T(k,q;\chi)\right]\right] \\ &= \frac{\kappa}{(2\pi)^3}\int \frac{d^3\mathbf{k}}{\tilde{E}^*(\mathbf{k})}\tilde{k}^{*\mu}k^\nu\Theta_{12}(k;\chi) \\ &- \frac{g^{\mu\nu}}{2}\frac{\kappa^2}{(2\pi)^6}\int \frac{d^3\mathbf{k}}{\tilde{E}^*(\mathbf{k})}\frac{d^3\mathbf{q}}{\tilde{E}^*(\mathbf{q})}\left[\tilde{M}^{*2}T_S(k,q;\chi) + \tilde{k}^*_\mu\tilde{q}^{*\mu}T_V(k,q;\chi)\right]\Theta_{12}(k;\chi)\Theta_{12}(q;\chi)\ . \end{aligned} \tag{17}$$

With eqs. (8-10) we express $T^{\mu\nu}$ in terms of the fields

$$T^{\mu\nu} =< \tilde{k}^{*\mu}k^{*\nu}/\tilde{E}^* >_{12} - V^{\mu\nu} - \frac{1}{2}g^{\mu\nu}\left\{\overline{\Sigma}_S\,\varrho_{S_{12}} - V^\lambda_\lambda\right\}\ . \tag{18}$$

The scalar contribution (12) and the terms containing the vector field are given by

$$V^{\mu\nu} =< \tilde{k}^{*\mu}\Sigma^\nu(k)/\tilde{E}^* >_{12}\quad . \tag{19}$$

The total scalar density and the total baryon current are given by

$$\varrho_{S_{12}} = -i\int \frac{d^4k}{(2\pi)^4}\mathrm{tr}\left[G_{12}(k)\right] =< \tilde{M}^*/\tilde{E}^* >_{12} \tag{20}$$

$$j_{\mu\,12} = -i\int \frac{d^4k}{(2\pi)^4}\mathrm{tr}\left[\gamma_\mu G_{12}(k)\right] =< \tilde{k}^*_\mu/\tilde{E}^* >_{12} \tag{21}$$

B. Mean field approximation

In order to examine the structure of the energy-momentum tensor (17) it is instructive to consider first the mean field approximation. To do so we use the Walecka model (QHD-I) [26]. In QHD-I the T-matrix amplitudes are replaced by corresponding coupling constants for a scalar σ and a vector ω meson field, $T_S \longmapsto \Gamma_S = g_\sigma^2/m_\sigma^2$ and $T_V \longmapsto \Gamma_V = g_\omega^2/m_\omega^2$, and thus the double integrals in (17) decouple. One could also use more sophisticated model such as density dependent hadron field theory [33] where $\Gamma_{S,V}(\varrho)$ are density dependent coupling functions. Such a density dependence can e.g. be taken from effective field theories [34] or again from the DB T-matrix [33]. In the latter case this provides the mean field approximation to the DB problem outlined above. In the following we consider the simpler case of constant couplings $\Gamma_{S,V}$ but the considerations can easily be generalized. Since the self-energies are now momentum independent one has $\tilde{k}^* = k^*$ and $\tilde{M}^* = M^*$. The energy-momentum tensor reads

$$T^{\mu\nu} =< k^{*\mu} k^{*\nu}/E^* >_{12} -\Gamma_V j_{12}^\mu j_{12}^\nu - \frac{1}{2} g^{\mu\nu} \left\{ \Gamma_S \varrho_{S_{12}} \varrho_{S_{12}} - \Gamma_V j_{12}^\lambda j_{\lambda\,12} \right\} \quad . \tag{22}$$

In nuclear matter one obtains the kinetic energy and pressure densities as

$$\epsilon_{\rm kin} = < E^*(\mathbf{k}) >= \frac{3}{4} E_F \varrho(k_F) + \frac{1}{4} M^* \varrho_S \tag{23}$$

$$p_{\rm kin} = \frac{1}{3} < \mathbf{k}^{*2}/E^* >= \frac{1}{4} E_F \varrho(k_F) - \frac{1}{4} M^* \varrho_S \quad . \tag{24}$$

The corresponding expressions in CNM are similar and transparent as long as the momentum distributions of the two currents do not overlap. Otherwise the contributions arising from the Pauli correction in (1) complicate the expressions considerably. Thus we first discuss the case where the relative velocity of the two currents is large enough to seperate the ellipsoids, i.e. $\Theta_1(k, u_1)\Theta_2(k, u_2) = 0$. The integrals for the kinetic energy density can be solved analytically and yield [8]

$$< k^{*\mu} k^{*\nu}/E^* >_{12}= g^{\mu\nu} \left\{ \frac{1}{4} M^* \varrho_{S_{12}} + \sum_{i=1,2} \frac{3}{4} E_{F_i} \varrho_0(k_{F_i}) \right\} - \sum_{i=1,2} \Delta_i^{\mu\nu} E_{F_i} \varrho_0(k_{F_i}) \tag{25}$$

Here $\varrho_0(k_{F_i})$ and $E_{F_i} = \sqrt{k_{F_i}^2 + M^{*2}}$ are the rest densities and the corresponding Fermi energies of the subsystems and $\Delta_i^{\mu\nu}$ is the projector (4) on the subsystem velocities. To further simplify (25) we consider symmetric configurations ($k_{F_{1,2}} = k_F, u_{1,2} = \pm u$). The total (c.m.) current is then given by $j_{\mu\,12} = j_{\mu\,1} + j_{\mu\,2} = (2\gamma(u)\varrho_0(k_F), \mathbf{0})$. Analogously the total scalar density reads

$$\varrho_{S_{12}} = \varrho_{S_1} + \varrho_{S_2} = 2\varrho_S(M^*) = \frac{2\kappa}{4\pi^2} M^* \left[k_F E_F - M^{*2} \ln\left(\frac{k_F + E_F}{M^*}\right)\right] \tag{26}$$

with $M^* = M - \Gamma_S \varrho_{S_{12}}$. Energy density $\epsilon = T^{00}$, transverse pressure $p_\perp = T^{11} = T^{22}$ and longitudinal pressure $p_\parallel = T^{33}$ are given by

$$\begin{aligned} T^{00} &= 2\left[\frac{3}{4} E_F \varrho_0(k_F) + \frac{1}{4} M^*\, \varrho_S(M^*) + E_F \varrho_0(k_F)\,(\gamma^2 - 1)\right] \\ &\quad + \frac{1}{2}\left\{\Gamma_V\,(2\gamma\varrho_0(k_F))^2 + \Gamma_S\,(2\varrho_S(M^*))^2\right\} \qquad (27) \\ p_\perp &= 2\left[\frac{1}{4} E_F \varrho_0(k_F) - \frac{1}{4} M^*\, \varrho_S(M^*)\right] \\ &\quad + \frac{1}{2}\left\{\Gamma_V\,(2\gamma\varrho_0(k_F))^2 - \Gamma_S\,(2\varrho_S(M^*))^2\right\} \qquad (28) \\ p_\parallel &= 2\left[\frac{1}{4} E_F \varrho_0(k_F) - \frac{1}{4} M^*\, \varrho_S(M^*) + E_F \varrho_0(k_F)\,(\gamma^2 - 1)\right] \\ &\quad + \frac{1}{2}\left\{\Gamma_V\,(2\gamma\varrho_0(k_F))^2 - \Gamma_S\,(2\varrho_S(M^*))^2\right\} \qquad (29) \end{aligned}$$

To compare CNM with NM it is instructive to rewrite Eqs. (27-29). The separation of projectile and target nucleons in momentum space increases the phase space volume in CNM. The boosted ellipsoids are elongated in longitudinal direction but in transverse direction the Fermi momenta k_F of the subsystems (which are fixed by the current rest densities $\varrho_0(k_F)$) are not enhanced. This feature can be accounted for if we integrate over one Fermi sphere at rest $\Theta(k; k_F, u = 0)$, however, with a doubled phase space occupancy factor 2κ

$$< X >_{2\kappa} = \frac{2\kappa}{(2\pi)^3} \int d^3\mathbf{k} X(k) \Theta(k; k_F, u = 0) \quad . \tag{30}$$

This description yields directly the CNM scalar density (26)

$$\varrho_{S_{12}} = < \frac{M^*}{E^*} >_{2\kappa} \tag{31}$$

and $2\varrho_0(k_F) =< 1 >_{2\kappa}$. One can now rewrite Eqs. (27-29) separating thereby the static parts from those contributions which depend on the streaming velocity. Making use of (30) the static parts of the energy and pressure densities are expressed as in ground state matter, however, with $\kappa = 8$:

$$T^{00} = T^{00}|_{2\kappa} + 2\gamma^2 \mathbf{u}^2 \left[E_F \varrho_0(k_F) + \Gamma_V \, \varrho_0^2(k_F) \right] \tag{32}$$

$$p_\perp = p_\perp|_{2\kappa} + 2\gamma^2 \mathbf{u}^2 \, \Gamma_V \, \varrho_0^2(k_F) \tag{33}$$

$$p_\parallel = p_\parallel|_{2\kappa} + 2\gamma^2 \mathbf{u}^2 \left[E_F \varrho_0(k_F) + \Gamma_V \, \varrho_0^2(k_F) \right] \tag{34}$$

Eqs. (32-34) are exact as long as the ellipsoids do not overlap. It can be directly seen from there that CNM is characterized by two effects which act in opposite direction: The first one is the separation of the nucleons belonging to the different currents in phase space. This effect acts like an additional degree of freedom. Evidently it reduces the pressure of the Fermi motion. Since the scalar part of the potential energy is not affected by the spread in momentum space, besides the fact that the contributions of projectile and target are superposed, it deepens the scalar potential. However, the vector repulsion gives rise to an additional velocity dependent pressure in both, transverse and longitudinal direction (terms proportional to Γ_V). The elongation of the boosted Fermi ellipsoids in longitudinal direction enhances the baryon vector density which leads to an additional kinetic pressure in longitudinal direction ($2\gamma^2 \mathbf{u}^2 E_F \varrho_0(k_F)$). Both these contributions are related to the kinetic energy of the relative motion in the system and enhance the energy density.

The comparison to equilibrated NM should be performed at identical rest densities, i.e. the two currents with their rest densities $\varrho_0(k_F)$ should be compared to NM at the same total density

$$\varrho_{NM}(k_{F_{tot}}) = 2\varrho_0(k_F) \quad ; \quad k_{F_{tot}} = 2^{\frac{1}{3}} k_F \quad . \tag{35}$$

By this procedure one prevents a distortion of the comparison by the purely kinematical enhancement of the boosted subsystem densities in the c.m. frame which does not affect the transverse degrees of freedom. A comparison of CNM and NM at identical total baryon

densities would mean to interpret the Lorentz contraction in the anisotropic system as a compression when related to the isotropic configuration. Condition (35) is also necessary for a meaningful comparison of CNM at different streaming velocities. Doing so, one can estimate the phase space effects comparing the contribution $T^{00}|_{2\kappa}(k_F)$ in (32) with $T^{00}|_{NM}(k_{F_{tot}})$ in NM. Schematically, the separation of phase space in the colliding system is illustrated in Fig. 1.

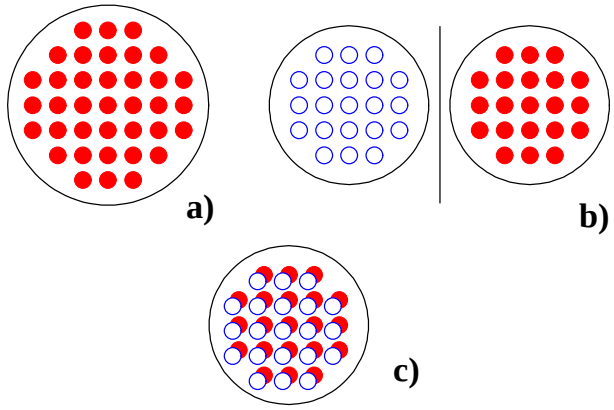

FIG. 1. Schematic representation of the phase space in nuclear matter (a), colliding nuclear matter (b), and in colliding nuclear matter as experienced by transverse degrees of freedom, respectively by the scalar, density dependent part of the interaction (c).

It is clear that the introduction of a new degree of freedom, e.g. going from neutron matter to isospin saturated matter, strongly increases the binding energy. In contrast to the scalar field, where the colliding configuration can be exactly treated by the introduction of an additional degree of freedom (Fig.1a$\mapsto$c), the vector field is enhanced by the spread in momentum space (Fig.1b) and the elongation of the boosted ellipsoids (not shown in Fig.1b). However, the present picture is more general. Besides the fact that in CNM the internal Fermi pressure of the subsystems is reduced also the contributions of the *internal* potential energy of the subsystems are modified due to the smaller Fermi momenta. The spread in momentum space, on the other hand, determines the interaction *between* the two currents and leads to additional repulsion in the combined system. These are the two essential features of colliding matter and - as will be seen later on - their implications on the EOS

are relatively independent on the choice of the nuclear forces.

The above considerations (Eqs. (26-34)) required that the ellipsoids were completely separated. The overlapping case which contains the limit $v_{\rm rel} \to 0$, i.e. equilibrated NM is more complicated. This involves the Pauli correction and the construction of the CNM configuration without double occupancy [8]. The principle of this procedure is to keep the streaming velocities u_i fixed and to enlarge the corresponding Fermi momenta ($k_F \to \tilde{k}_F$) thus that the condition

$$\begin{aligned} j_{0\,12}(\tilde{k}_F) &= \frac{\kappa}{(2\pi)^3}\int d^3k \left[\Theta_1(k;\tilde{k}_F,u) + \Theta_2(k;\tilde{k}_F,-u) - \Theta_1(k;\tilde{k}_F,u)\Theta_2(k;\tilde{k}_F,-u)\right] \\ &= 2\gamma(u)\varrho_0(k_F) \end{aligned} \tag{36}$$

is fulfilled. Eq. (36) is valid for the symmetric case but can easily be extended to asymmetric configurations [8]. In the mean field approximation the integrals over the intersection ellipsoids can be worked out analytically which has been done by L. Sehn [20]. For the energy density one ends up with

$$\begin{aligned} T^{00} &= \frac{1}{4}M^*(\tilde{k}_F)\,(2\varrho_S(\tilde{k}_F) - \delta\varrho_S) \\ &+ \frac{1}{2}\left\{\Gamma_V\,\gamma^2(2\varrho_0(\tilde{k}_F) - \delta\varrho_0)^2 + \Gamma_S\,(2\varrho_S(\tilde{k}_F) - \delta\varrho_S)^2\right\} \\ &+ \frac{\kappa}{8\pi^2}\left\{-\frac{1}{2}M^{*4}\ln\left[\sqrt{\frac{1+u}{1-u}}\frac{\tilde{E}_F - \tilde{k}_F}{M^*}\right]\right. \\ &- \tilde{k}_F\tilde{E}_F M^{*2} + \frac{1}{3u}\gamma^2\tilde{E}_F(\tilde{E}_F - u\tilde{k}_F)^3 - \frac{1}{3u}\left(\frac{\tilde{E}_F}{\gamma}\right)^4 \\ &\left.- \frac{1}{2}\gamma^2 M^{*2}(u\tilde{E}_F - \tilde{k}_F)(\tilde{E}_F + u\tilde{k}_F)\right\} \quad . \end{aligned} \tag{37}$$

The Pauli correction terms $\delta\varrho_S$ and $\delta\varrho_0$ (originating from the $\Theta_1\Theta_2$ overlap integrals) can be found in [8]. In the limit $u \to 0$ the CNM configuration (1) approaches smoothly the corresponding NM configuration $\Theta(k_{F_{tot}})$ with $\tilde{k}_F \to k_{F_{tot}}$, $\delta\varrho_S(\tilde{k}_F) \to \varrho_S(k_{F_{tot}})$ and $\delta\varrho_0(\tilde{k}_F) \to \varrho_0(k_{F_{tot}})$. The same holds for the energy momentum tensor, i.e. $T^{\mu\nu}(\tilde{k}_F, u \to 0) \to T^{\mu\nu}(k_{F_{tot}}, u = 0)$. The enhancement factor which accounts in (26-34) effectively for the enlarged phase space volume approaches unity, i.e. $2\kappa \to \kappa$.

III. THE EFFECTIVE EOS

In colliding nuclear matter the energy per particle is defined in the usual way

$$E_{12}(\varrho_{12}, u) = \mathrm{T}^{00}/\varrho_{12} - M \tag{38}$$

with $\varrho_{12} = \sqrt{j_{12}^2}$ the invariant baryon density in the c.m. frame of the two currents. [1] However, a meaningful discussion of non-equilibrium effects with respect to the ground state EOS should be based on the binding energy per particle. In the temperature zero case this corresponds to the free energy of the system where the contribution from the relative motion of the two currents has been subtracted. The corresponding effective EOS in colliding matter is then also directly linked to the hydrodynamical picture [1]. The kinetic energy of a nucleon inside the medium is given by $E^*_{\rm kin} = E^*(k) - M^*(k)$. Analogously, we identify the kinetic energy density of the relative motion in (18) with

$$\mathcal{E}_{\rm kin} =< \tilde{k}^{*0}(k^{*0} - M^*)/\tilde{E}^* >_{12} =< E^*(k) - M^*(k) >_{12} \quad . \tag{39}$$

The effective mass M^* accounts in (39) for the fact that the two currents are interacting by momentum dependent forces. Such a momentum dependence occurs in the relativistic treatment already on the mean field level where the self-energies do not explicitely depend on momentum. The magnitude of M^* characterizes thereby the strength of the momentum dependence of the optical potential. On the other hand side, different parameterizations of QHD including additional non-linear self-interaction terms for the scalar σ field [27] can yield identical EOSs but differ in their momentum dependence. This effect is taken into account in (39). Moreover, the kinetic energy equals $E^* - M^* \simeq \frac{\mathbf{k}^2}{2M^*}$ in the non-relativistic

---

[1] According (36) the c.m. density is related to the subsystem rest densities by $\varrho_{12} = 2\gamma(u)\varrho_0(k_F)$. To avoid the stretching of the density scale by the Lorentz contraction we will in the following represent the energy density as a function of the subsystem rest densities $2\varrho_0(k_F)$. Physically this means to remove the Lorentz contraction in the representation of the free energy.

limit. In the non-relativistic limit M^* plays the role of the Landau mass which is used to parameterize the optical potential.

The energy of the relative motion of two interacting currents is more subtle to define. The present description is inspired by the fact that in the non-relativistic case this should be the energy which is necessary to shift the two Fermi spheres in their c.m. frame against each other. In the relativistic framework this corresponds to the difference of the kinetic energy in the combined system and the corresponding NM configuration at twice the subsystem rest density $2\varrho(k_F)$

$$\mathcal{E}_{\rm rel}(k_F,u) =< E^* - M^* >_{12} - < E^* - M^* >_{u=0} \quad . \tag{40}$$

By definition $\mathcal{E}_{\rm rel}$ contains the kinetic energy which arises from the separation of the two distributions, respecting thereby the Pauli principle, and accounts for the interaction between the two currents by the presence of the effective mass. The vector density is not conserved when boosting the two distributions against each other. The Lorentz contraction contributes therefore to the energy of the relative motion. Similar as the c.m. energy density ($\epsilon = T^{00}|_{\rm c.m.} = u_\mu T^{\mu\nu} u_\nu$), Eq. (40) can be formulated in an invariant manner

$$\begin{aligned}\mathcal{E}_{\rm rel}(k_F,u) = u_{12\,\mu} < \tilde{k}^{*\mu}(k^{*\nu} - M^*\delta_0^\nu)/\tilde{E}^* >_{12} u_{12\,\nu} \\ -u_{1\,\mu} < \tilde{k}^{*\mu}(k^{*\nu} - M^*\delta_0^\nu)/\tilde{E}^* >_{1} u_{1\,\nu} \quad .\end{aligned} \tag{41}$$

Now one obtains the binding energy per particle

$$E_{12}^{\rm bind}(k_F,u) = \frac{T^{00} - \mathcal{E}_{\rm rel}}{\varrho_{12}} - M \tag{42}$$

as a function of the total c.m. density ϱ_{12} and the c.m. streaming velocities. In the following we will only consider symmetric configurations ($k_{F_{1,2}} = k_F, u_{1,2} = \pm u$). The basic features of the colliding configuration are easier discussed at the mean field level where formulas have been evaluated analytically and thus we consider this case first.

A. Mean field approximation

Here we mainly use the QHD-I version of the Walecka model with only two free parameters adjusted to the nuclear matter bulk properties. The model yields a binding energy of -15.75 MeV, a relatively large saturation density ($k_{F_{\rm sat}} = 1.42$ fm^{-1}), a small effective mass of M^*/M=0.556 and a large compression modulus of K=540 MeV.

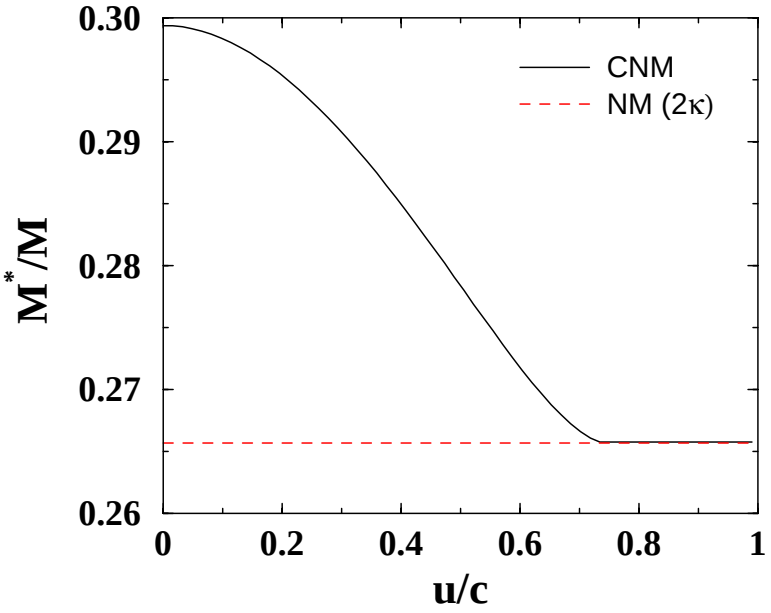

FIG. 2. Effective mass in colliding nuclear matter (CNM) at subsystem densities $\varrho_0 = \varrho_{\rm sat}$ as a function of the streaming velocity (solid) compared to the corresponding effective mass in nuclear matter obtained at ϱ_0 with a doubled phase space factor (2κ, dashed). Results are obtained with the Walecka model QHD-I.

To illustrate the influence of the two-current geometry on the scalar part of the interaction in Fig. 2 the effective mass in colliding nuclear matter at subsystem densities $\varrho_{\rm sat}$ is shown as a function of the streaming velocity. At zero velocity the nuclear matter result at twice saturation density ($\varrho = 2\varrho_{\rm sat}$) is obtained. With increasing streaming velocities the effective mass drops and reaches around $u/c = 0.7$ (which corresponds to $E_{\rm lab}$=1.8 GeV) the asymptotic value of the non-overlapping configuration given by expression (26). A further increase of u has no influence on the effective mass since the scalar densities can be evaluated

in the local rest frames of the currents. At the mean field level M^* is exclusively determined by the shape of the momentum distribution, but once the ellipsoids are separated, the effective mass stays constant. The asymptotics are given by the corresponding effective mass in nuclear matter at ϱ_0 with the enlarged phase space factor (2κ). Hence the two-ellipsoid geometry enhances the attractive scalar field by about 30 MeV. However, in the total energy per particle (38) this enhancement is completely compensated by the additional repulsive contributions in the counter-streaming system. As discussed above, Eqs. (32-34), an additional longitudinal Fermi pressure occurs due to the boosted vector densities. Secondly, the vector field gives rise to a strong repulsive force between the two currents.

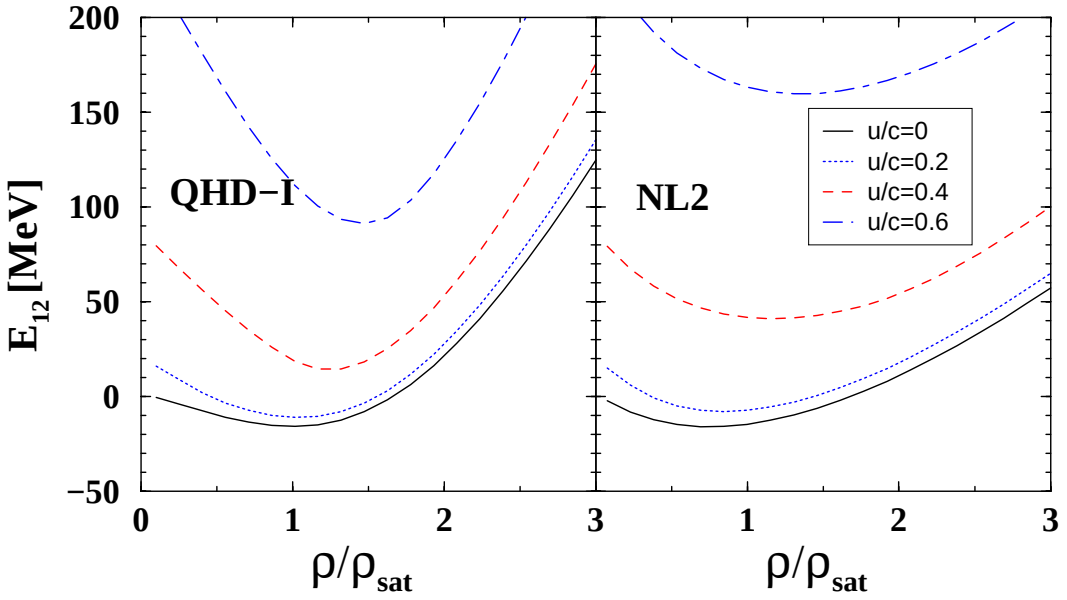

FIG. 3. Energy per particle E_{12} in colliding nuclear matter as a function of the subsystem density $2\rho_0/\varrho_{\rm sat}$ at different streaming velocities u/c=0/0.2/0.4/0.6. Results are obtained with the Walecka model QHD-I (left) and the non-linear Walecka model NL2 (right). In both cases densities are normalized to the saturation density $\varrho_{\rm sat} = 0.193$ fm^{-3} of QHD-I.

As can be seen from Fig. 3 the additional scalar attraction in the total energy per particle (38) is then completely hidden by the much stronger repulsive contributions. Already at very low streaming velocities the system appears to be unbound. One should, however, be

aware that QHD-I is a model with an unrealistically strong repulsive character at higher momenta, expressed by its small effective mass and the large vector field. As a result QHD-I strongly over predicts the empirical optical nucleon-nucleus potential [35] and the transverse nucleon flow in heavy ion collisions [9,36]. To estimate the model dependence inherent in the present considerations in Fig. 3 we compare also to a softer version, the non-linear Walecka model NL2 [37], with bulk properties of $E = -15.75$ MeV, $k_{F_{\rm sat}} = 1.29$ fm^{-1}, K=237 MeV. A large effective mass M^*/M=0.80, respectively a weaker momentum dependence leads to a more realistic description of the dynamics in heavy ion reactions [9,36]. Although less repulsive at large momenta the NL2 parameterization yields qualitatively the same velocity dependence of the total energy per particle as QHD-I.

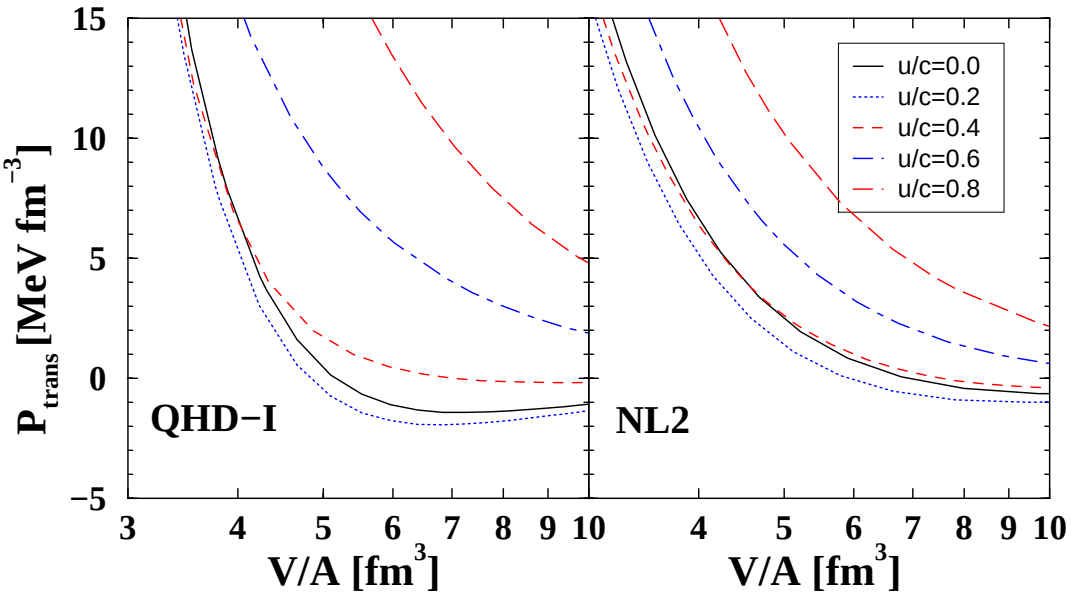

FIG. 4. Transverse pressure $p_\perp$ in colliding nuclear matter as a function of the volume per particle at different streaming velocities. Results are obtained with the Walecka model QHD-I (left) and the non-linear Walecka model NL2 (right).

In Fig. 4 the transverse pressure $p_\perp = T^{11} = T^{22}$ is shown as a function of the volume per particle $V/A = 1/\varrho_{12}$. Interestingly, the transverse pressure is reduced at low streaming velocities. Although the momentum distribution of the two currents is still quite compact at

$u/c = 0.2$ the reduction of the Fermi pressure and the reduction of the effective mass by the enlarged phase space volume are sufficient to produce this softening in transverse direction. However, with increasing velocity the vector repulsion starts to dominate. Qualitatively this behavior is model independent, i.e. it occurs in QHD-I and the softer NL2 model. Only at the highest velocity shown in Fig. 4 ($u/c = 0.8$) the ellipsoids are well separated, i.e. eq. (33) is exactly valid. At smaller u the Pauli corrections are taken into account.

In order to investigate the subtle features of the colliding system we consider now the effective binding energy per particle (42). With eq. (25) the energy of the relative motion can easily be evaluated in mean field approximation (no overlap):

$$\begin{aligned}\mathcal{E}_{\rm rel} = 2\varrho_0(k_F)\left[E_F\left(\gamma^2 - \frac{1}{4}\right) - \frac{3}{4}E_{F_{\rm tot}} - \gamma M^* + M^*(k_{F_{\rm tot}})\right] \\ + \frac{1}{4}\left[M^*\varrho_{S\,12} - M^*(k_{F_{\rm tot}})\varrho_S(k_{F_{\rm tot}})\right] \quad .\end{aligned} \tag{43}$$

The meaning of (43) becomes more transparent in the low density limit. Using

$$\varrho_S = \varrho_0\left[1 - \frac{3}{10}\left(\frac{k_F}{M^*}\right)^2 + \mathcal{O}\left(\left(\frac{k_F}{M^*}\right)^4\right)\right] \tag{44}$$

one obtains after an expansion in u/c

$$\mathcal{E}_{\rm rel} = 2\varrho_0(k_F)\left[\frac{M^*}{2}u^2 + \frac{3}{5}\frac{k_F^2}{2M^*} + \frac{k_F^2}{2M^*}u^2 - \frac{3}{5}\frac{k_{F_{\rm tot}}^2}{2M^*(k_{F_{\rm tot}})}\right] + \mathcal{O}(u^4) \quad . \tag{45}$$

Now it becomes evident that eq. (45) contains the kinetic energy of two freely streaming gases $T^{00} - \gamma M^*\varrho_0$. The first term is just the mean kinetic energy of a comoving nucleon, the second term is the kinetic energy of the internal Fermi motion in the local rest frame and the third contribution is due to the elongation of the Fermi ellipsoids in longitudinal direction by the boosts. Subtracted is the kinetic energy of the Fermi motion of the rest system at equal rest densities. Hence the definition (43) respects the Pauli principle. An alternative choice would be to subtract simply the kinetic energy of the superimposed two spheres as illustrated by Fig. 1c which would, however, violate the Pauli principle. To subtract the kinetic energy of the rest system at identical, Lorentz enhanced vector densities, on the other hand side, would introduce an additional unreasonable velocity dependence into the

last term of eq. (45). Thus eq. (40) is the natural definition of the relativistic kinetic energy of the relative motion and contains the correct non-relativistic limit.

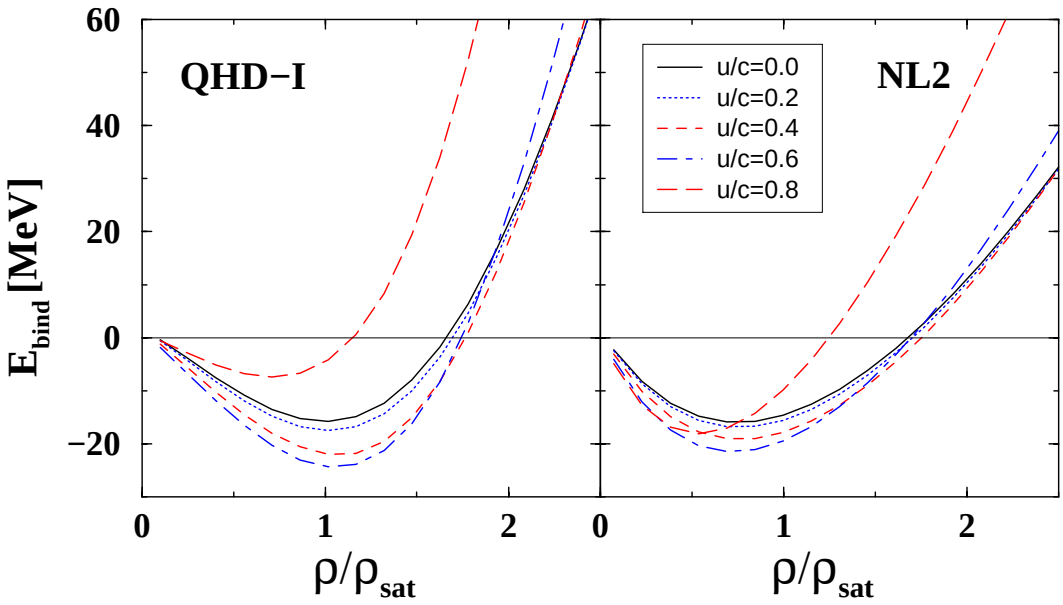

FIG. 5. Effective binding energy per particle $E_{12}^{\rm bind}$ in colliding nuclear matter as a function of the subsystem density $2\rho_0/\varrho_{\rm sat}$ at different streaming velocities. Results are obtained with the Walecka model QHD-I (left) and the non-linear Walecka model NL2 (right). In both cases densities are normalized to the saturation density $\varrho_{\rm sat}$ of QHD-I.

Now one is able to construct an effective EOS which relates colliding to ground state matter. In Fig. 5 the corresponding effective equations of state are shown. First of all it is seen that the two-Fermi-ellipsoid geometry leads to a softening of the effective EOS at moderate streaming velocities. This can be understood by the reduced Fermi pressure in transverse direction and the enlarged scalar attraction as compared to NM. The vector potential is not affected by the subtraction scheme for $\mathcal{E}_{\rm rel}$ and contributes fully to $E_{12}^{\rm bind}$. Thus, the enhancement of the vector repulsion acts in opposite direction and makes the EOS harder at large densities and/or high streaming velocities. Here the model dependences become more significant. At $u/c = 0.8$ the effective QHD-I EOS lies well above the corresponding ground state result whereas for NL2 it is still softer at low densities. This reflects nicely the

weaker momentum dependence and the weaker repulsion of NL2. In summary the softening of the "'effective EOS"' by about 10 MeV due to the anisotropic phase space distributions in CNM is hardly seen on the scale of the total energy per particle but on the scale of an effective binding energy. Such small effects are, however, the features one is after in heavy ion experiments at intermediate energies.

B. DB approximation

The mean field used in the present section is based on recent DB calculations [29] with nuclear matter saturation properties (Bonn A potential) of $\rho_{\rm sat} = 0.185$ fm^{-3}, $E^{\rm bind} = -16.15$ MeV, a compression modulus of $K = 230$ MeV and an effective mass of $\tilde{M}^*/M = 0.678$ which lies in between the phenomenological models QHD-I and NL2. In ground state matter the momentum dependence of the DB self-energies is moderate above the Fermi surface. The solution of the full DB problem for colliding nuclear matter, i.e. the self-consistent solution of the BS-equation for two-Fermi-ellipsoid configurations, is still an unresolved problem. Thus we determine the effective interaction in CNM as described in [8]. The ground state T-matrix amplitudes are parameterized in form of averaged momentum and density dependent scalar and vector coupling functions

$$\bar{T}_S(k;k_F) = \int \frac{d^3\mathbf{q}}{\tilde{E}^*(\mathbf{q})} \tilde{M}^* T_S(k,q;k_F)\ \Theta(q;k_F)\ /\ \int \frac{d^3\mathbf{q}}{\tilde{E}^*(\mathbf{q})} \tilde{M}^*\ \Theta(q;k_F) \tag{46}$$

$$\bar{T}_V(k;k_F) = \int \frac{d^3\mathbf{q}}{\tilde{E}^*(\mathbf{q})} T_V(k,q;k_F)\ \Theta(q;k_F)\ /\ \int \frac{d^3\mathbf{q}}{\tilde{E}^*(\mathbf{q})}\ \Theta(q;k_F)\ \ . \tag{47}$$

The amplitudes $T_{\rm S,V}$ in eqs. (16,17) should self-consistently be determined for colliding matter configurations. However, in the present work they are approximated by the corresponding NM amplitudes $\bar{T}_{\rm S,V}$, read in the subsystems at the respectively transformed momenta k'. Details of this procedure can be found in [8]. The treatment is not self-consistent on the level of the effective two-body interaction, e.g. the influence of the anisotropic momentum configuration on the Pauli operator for the intermediate states in the BS-equation is not taken into account, but it accounts for the correct geometry and the integration of the

T-matrix amplitudes over this geometry. Fig.6 displays the momentum dependence of the $\bar{T}_{\mathrm{S,V}}$ amplitudes at various densities. At high momenta which exceed the range of the DB calculations we assume a $1/k$ asymptotics for the amplitudes.

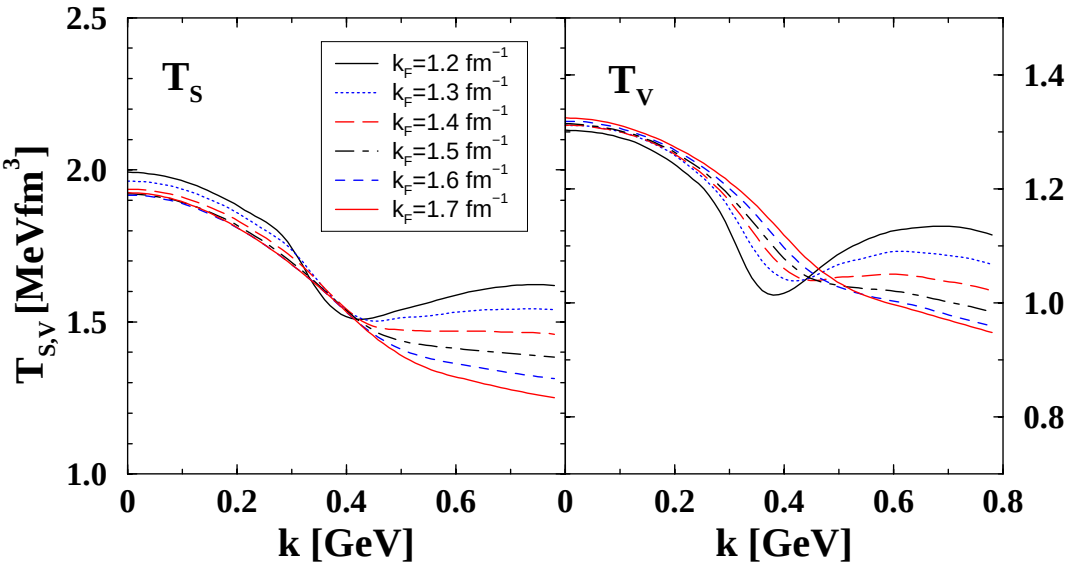

FIG. 6. Averaged scalar and vector T-matrix amplitudes $\bar{T}_{\mathrm{S,V}}$ at various densities. The amplitudes are obtained from DB calculations for NM at rest.

The corresponding equations-of-state are shown in Fig.7. The behavior of both, the energy per particle E_{12} and the effective binding energy per particle E_{12}^{bind} are similar to the MF models discussed above. As already expressed by the saturation properties the DB model is significantly less repulsive than QHD-I. Moreover, the explicit density and momentum dependence of the amplitudes $\bar{T}_{\mathrm{S,V}}$ leads to some visible deviations from the MF picture. At low streaming velocities ($u = 0.2,\ 0.4$) even the total energy E_{12} lies slightly below the ground state result. Consequently, the increase in binding energy seen in the effective EOS (lower part of Fig.7) is more pronounced than in the MF approach, in particular at high densities. This behavior is due to the fact that the amplitudes $\bar{T}_{\mathrm{S,V}}$ decrease with density and momentum. Compared to the MF case this momentum dependence leads to a reduction of both, the scalar and the vector field. In particular the reduction of the vector field, which

increases in the MF models linearly with γ and ϱ, results in considerably less repulsion for highly anisotropic CNM configurations.

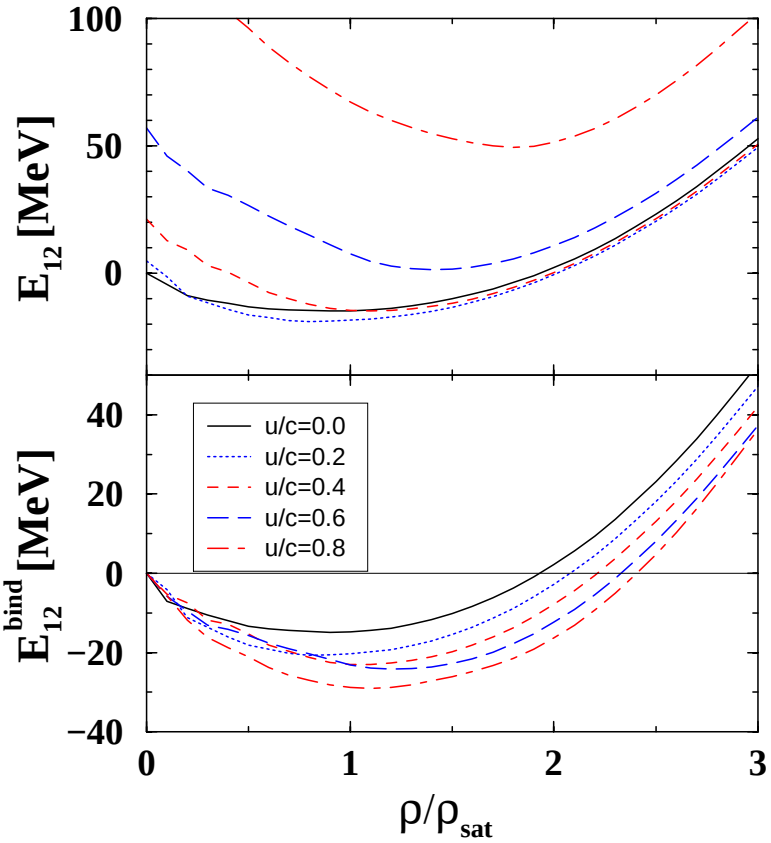

FIG. 7. EOS in nuclear matter (solid) and colliding nuclear matter as a function of the subsystem density $2\rho_0/\varrho_{\rm sat}$ at different streaming velocities. The DB model is used. The upper and lower parts show the total energy per particle E_{12} and the effective EOS, i.e. the binding energy per particle $E_{12}^{\rm bind}$ where the kinetic energy of the relative motion in CNM has been subtracted, respectively. The streaming velocities are u=0.2 (dotted), 0.4 (dashed), 0.6 (long-dashed), 0.8 (dot-dashed). In both cases densities are normalized to the saturation density $\varrho_{\rm sat}$ the DB model.

The momentum dependence of the T-matrix amplitudes is also reflected in the configuration dependence of the effective mass $\tilde{M}^*$ shown in Fig.8 as a function of the streaming velocity at fixed subsystem densities $\varrho_0 = \varrho_{\rm sat}$. As in the MF approximation, $\tilde{M}^*$ drops first with increasing anisotropy but does not fully reach the limit of a doubled phase space factor (2κ). Instead, $\tilde{M}^*$ starts to rise again at high relative velocities. This reflects the

decrease of the scalar amplitude at large momenta, respectively the reduction of the scalar field when the momentum integration over the configuration is performed. In summary, the DB model follows to large extent the behavior of the MF approach. The leading kinematical effects such as the separation of phase space and a dropping effective mass as a function of the anisotropy are present. Superimposed are the density and momentum dependence of the T-matrix amplitudes. The explicit momentum dependence of the effective interaction leads to a reduced strength of both, the scalar and the vector field at large relative momenta which results in an even softer effective EOS in CNM compared to the MF picture.

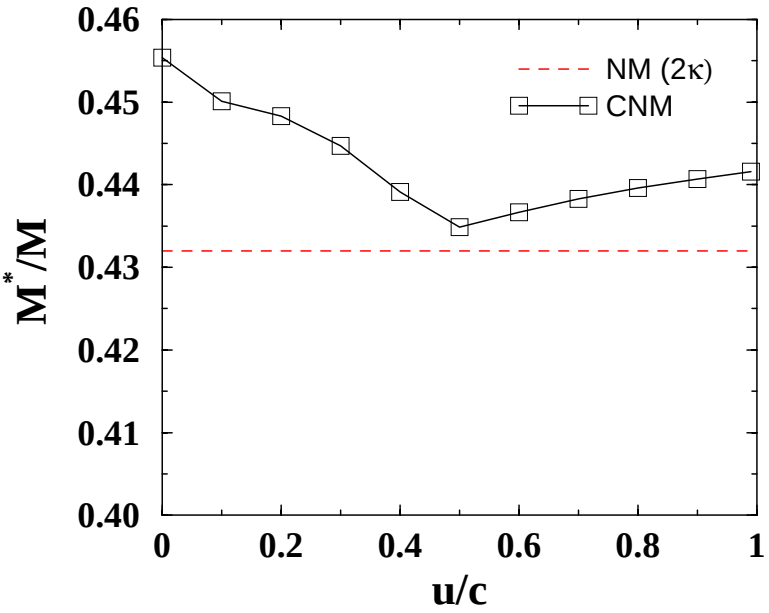

FIG. 8. Effective mass in colliding nuclear matter (CNM) at subsystem densities $\varrho_0 = \varrho_{\rm sat}$ as a function of the streaming velocity in the DB model. The result is compared to the corresponding effective mass in nuclear matter obtained at ϱ_0 with an enlarged phase space factor (2κ, dashed).

IV. HEAVY ION REACTIONS

In this section the connection of the previous considerations with transport calculations is discussed. The early and high density phase of relativistic heavy ion reactions in the SIS ($E_{\rm lab} < 2$ AGeV) and AGS ($E_{\rm lab} < 10$ AGeV) energy range are characterized by a

high anisotropy of the local momentum space in beam direction. This has also practical implications for heavy ion reactions and the interpretation of experimental observables. In the overlapping zone of two interpenetrating nuclei the initial configuration is that of two sharp momentum ellipsoids. In the course of the reaction the mid-rapidity region is then more and more populated due to binary collisions and the system is heated up, i.e. the originally cold and sharp momentum ellipsoids become diffuse and merge together. At least in the central cell finally a fully equilibrated spherical configuration can be reached. This has e.g. been demonstrated in [11–13].

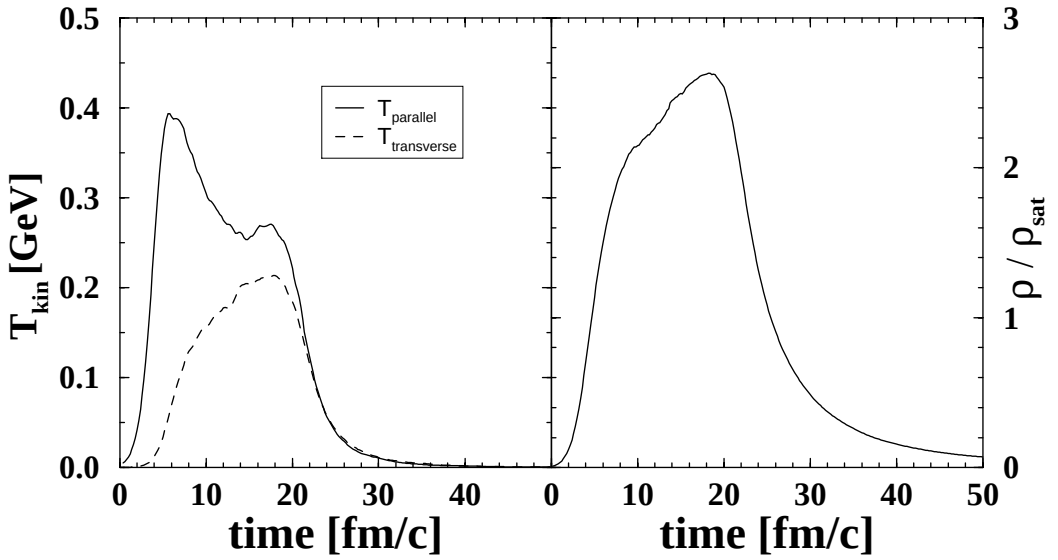

FIG. 9. Time evolution of the kinetic part of the energy-momentum-tensor $T_{\rm kin}$ (left) and the baryon density (right) at the collision center in a central $Au+Au$ reaction at 1 A.GeV. The tensor components parallel $T^{\parallel}_{\rm kin}$ and transverse $T^{\perp}_{\rm kin}$ to the beam direction are shown separately.

To obtain a more quantitative measure for the size and relevant time scales for phase space anisotropies in Fig.9 the time evolution of the kinetic part of the energy-momentum-tensor at the collision center of a central (b=0 fm) $Au+Au$ reaction at 1 A.GeV is compared to the time evolution of the corresponding baryon density. The difference between the parallel $T^{\parallel}_{\rm kin} = T^{33}_{\rm kin}$ and the transverse $T^{\perp}_{\rm kin} = (T^{11}_{\rm kin}+T^{22}_{\rm kin})/2$ components is thereby a measure

for the anisotropy of the local momentum space in beam (z) direction. The quantities are obtained from relativistic BUU calculations where $T^{\mu\nu}_{\rm kin}$ is determined from the phase space distribution $f(\mathbf{x},\mathbf{k},t)$ represented by testparticles [25]

$$T^{\mu\nu}_{\rm kin}(\mathbf{x},t) =< k^{*\mu}k^{*\nu}/E^* >_f = \frac{1}{N}\sum_i^{A\cdot N} u_i^\mu u_i^\nu m_i^* g(\mathbf{x},\mathbf{x}_i,t)\ . \tag{48}$$

The index i in Eq.(48) refers to the testparticle and g is a covariant Gaussian [25]. In the initial phase up to about 10 fm/c the local phase space is highly anisotropic, i.e. $T^{\parallel}_{\rm kin} >> T^{\perp}_{\rm kin}$. During the high density phase from $\sim\ 5 \div 25$ fm/c the system starts to equilibrate. At the end of the high density phase and during the expansion phase the two components of the energy-momentum tensor are almost equal which indicates that a large amount of equilibration has been reached. Fig.9 demonstrates also that the relaxation time to reach equilibrium configurations ($T^{\parallel}_{\rm kin} = T^{\perp}_{\rm kin}$) coincides more or less with the high density phase of the reaction.

Now the question arises how accurately the BUU phase space can be reproduced by a sequence of colliding nuclear matter configurations. It is clear that the considered CNM configurations are an idealization of the real phase space. Firstly, one assumes symmetric configurations in projectile and target currents whereas the transport simulations contain density fluctuations. Secondly, the system is heated up whereas temperature effects are neglected in the cold configurations. To estimate the validity of this approximation the following procedure is applied:

The temporal evolution of the two parameters $\varrho_0 = \varrho_0^T + \varrho_0^P$ and $v_{\rm rel}$ which characterize the anisotropic momentum space in terms of CNM are directly determined from the RBUU simulation, again in the central cell for Au+Au at 1 AGeV. The effective compression density ϱ_0 is given as the sum of the projectile and target invariant rest densities $\varrho_0^{T/P} = \sqrt{j_\mu^{T/P} j^{\mu T/P}}$ and the velocity $v_{\rm rel} = |\mathbf{v}_{\rm rel}|$ is defined via the projectile and target streaming velocities

$$\mathbf{v}_{\rm rel} = \frac{u_0^T\mathbf{u}^P - u_0^P\mathbf{u}^T}{u_\mu^T u^{P\mu}}\quad . \tag{49}$$

These values are compared to the corresponding $\varrho_0, v_{\rm rel}$ parameters for idealized symmetric ($\varrho_0^T = \varrho_0^P$) CNM configurations. Here $v_{\rm rel}$ is chosen in such a way that at given ϱ_0 the

kinetic energy-momentum tensor components $T^{\parallel}_{\rm kin}, T^{\perp}_{\rm kin}$ from the transport simulations are reproduced. The comparison is performed in Fig. 10 where each symbol corresponds to a time step of $\Delta t = 0.2$ fm/c. Although not perfect, the CNM approximation is able to describe the time evolution in the $\varrho_0 - v_{\rm rel}$ parameter space quite well. Since the CNM parameters are adjusted to reproduce the kinetic energy, deviations in the $v_{\rm rel}$ parameter can be regarded a measure for the difference between the real and the idealized configurations. These are due to temperature and finite size effects as well as to asymmetries arising from density fluctuations. One has thereby, however, to keep in mind that a description in terms of a naive local density approximation would completely neglect the dependence on the $v_{\rm rel}$ parameter.

From the time evolution of the system in the $\varrho_0 - v_{\rm rel}$ parameter space the following can be seen: Asymptotically the two nuclei start to touch at low density and high $v_{\rm rel}$. Then the density increases rapidly and reaches a maximum value of about 2.5 $\varrho_{\rm sat}$. In the beginning $v_{\rm rel}$ is large but then equilibration sets in. When maximal compression is reached the relative velocity is still relative high ($v_{\rm rel}/c \simeq 0.6$), i.e. the local momentum space is still highly anisotropic. In the expansion phase the density drops rapidly and the system becomes more and more isotropic. Interestingly, the system stays for some time in the region of highest compression before it expands, i.e. it takes some time before an isotropic pressure builds up. Also in [12] it was found that only in the final expansion phase the pressure is isotropic. Thus the momentum space anisotropy is most distinct before maximal compression is reached, consistent with Fig. 9. One effect which should also be noted is the slight increase of $v_{\rm rel}$ in the first two fm/c. This acceleration is a typical effect due to the interaction between the two currents. In the interacting system the effective mass drops which leads to the slight acceleration before the stopping due to binary collisions sets in.

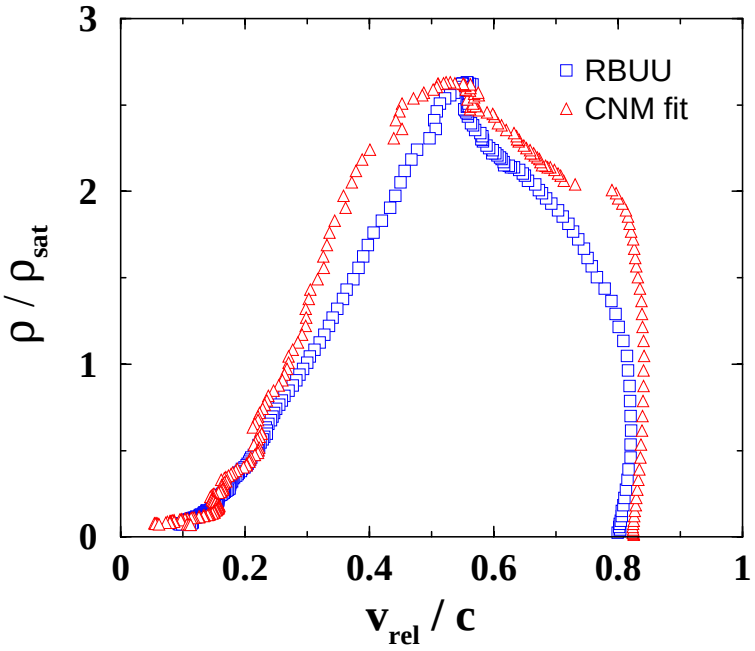

FIG. 10. Time evolution of the two parameters, total density ϱ_0 and relative streaming velocity $v_{\rm rel}$, which characterize anisotropic momentum configurations. The squares denote the values obtained in the central cell from a RBUU calculation for a central $Au + Au$ reaction at 1 AGeV. The triangles are the values determined by adjusting colliding nuclear matter configurations to the kinetic energy distributions of the RBUU calculation. Each symbol corresponds to a time step of 0.2 fm/c.

Thus one sees that the picture of two counter-streaming fluids is appropriate for a major part of the reaction, in particular when supra-normal densities are present. Certainly the assumption of cold fluids has to be improved since the system is heated up. However, with respect to the local density approximation where the $v_{\rm rel}$ dependence is to large extent neglected in the determination of the mean field the two-fluid picture provides an important step forward towards a more precise dependence of the mean field on the phase-space configuration. In transport calculations like BUU [22] or QMD [10] or their relativistic counterparts RBUU [9,25] and RQMD [36] the mean field is usually determined in a sort of a local density approximation. In the simplest approximation where no explicit momentum dependent forces are considered the fields depend only on the total density. In a non-relativistic

approach this yields a local potential of the Skyrme type $U_{\rm s.p.} = \alpha\rho_B + \beta(\rho_B)^\gamma$. In the relativistic case the single particle potential has the form

$$U_{\rm s.p.}(\rho_B, k) = k^0 - \sqrt{M^2 + \mathbf{k}^2} = \sqrt{\mathbf{k}^{*2} + M^{*2}} - \Sigma_0 - \sqrt{M^2 + \mathbf{k}^2} \quad . \tag{50}$$

In mean field approximation, i.e. for Walecka type models, the scalar and vector fields depend on the local density, i.e. $M^* = M + \Sigma_S(\rho_B)$, $\Sigma_0 = \Sigma_0(\rho_B)$ and the lowest order momentum dependence of $U_{\rm s.p.}$, which is absent in non-relativistic treatments, originates from the difference between M and M^*. It is worthwhile to extract the error which is made when the local density approximation (LDA) is applied to anisotropic momentum space configurations. Naturally, the LDA accounts only insufficiently for such a scenario. In transport simulation the particles are usually propagated in the center-of-mass frame of the colliding nuclei which corresponds to the c.m. frame of the two counter-streaming currents. There the baryon density is given by $\rho_B = \varrho_{12} = 2\gamma\varrho_0$ which means that the LDA treats the Lorentz contraction of the nuclei like a compression.

To estimate the resulting error in the dynamics we compare the correct single particle potential for CNM to that obtained by making use of the LDA. Therefore a typical nucleon comoving with one of the currents with its average velocity u is chosen. In the c.m. frame the spatial components of the total current j_{12} vanish and the vector field contains only the time like component. Hence the momentum of such a "test" nucleon is given by $\mathbf{k} = \mathbf{k}^* = M^*\gamma u\hat{e}_z$. Since the vector fields is on the mean field level identical in both, the CNM calculation and using the LDA, i.e. $\Sigma_0 = \Gamma_V\varrho_{12} = \Gamma_V\rho_B$, differences in the single particle potential arise only due the different values of the effective mass.

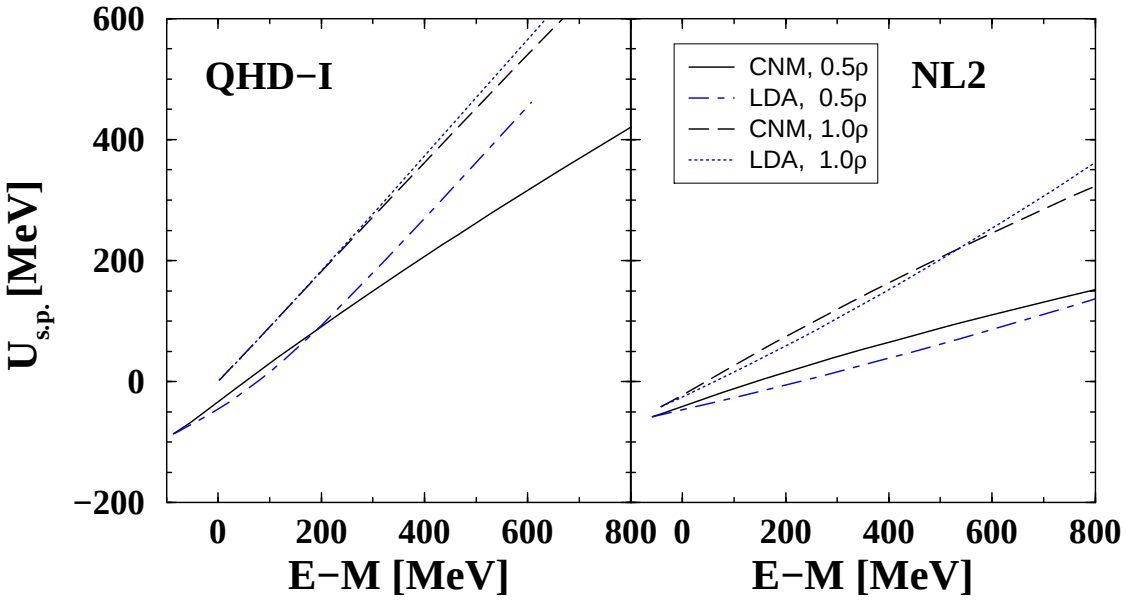

FIG. 11. Single particle potential in colliding nuclear matter for a test nucleon which is comoving with one of the currents at subsystem rest densities of 0.5 and 1.0 $\varrho_{\rm sat}$. The CNM calculation is compared to the local density approximation. Results are obtained with the Walecka model QHD-I (left) and the non-linear Walecka model NL2 (right).

In Fig. 11 the single particle potential (50) for such a test nucleon moving with streaming velocity u is shown as a function of the single particle energy $E_{\rm s.p.} = k^0 - M$, for the two subsystem densities $\varrho_0 = 0.5\varrho_{\rm sat}$ and $1.0\varrho_{\rm sat}$. In this representation both, $E_{\rm s.p.}$ and the baryon density $\rho_B = 2\gamma\varrho_0$ depend on u. The effective mass and the resulting nucleon momentum are consistently determined for the colliding configuration (including Pauli effects). We compare this to the LDA where the fields are determined as for ground state nuclear matter at ρ_B. Due to the different value for M^* one obtains a different test nucleon momentum at fixed u. As seen from Fig.11 the LDA leads to significant deviations in the single particle potential. That the deviations are even more pronounced at lower densities ($0.5\varrho_{\rm sat}$) comes from the fact that at high densities the potential is dominated by the vector field which coincides in the two approaches. Comparing QHD-I and NL2 illustrates the model dependence of the error made by the LDA. At higher energies the LDA predicts generally a too repulsive potential,

at low energies on the other hand too much attraction. The reason lies in the interplay between M^* and k which both enter into $U_{\rm s.p.}$ and $E_{\rm s.p.}$. For increasing streaming velocities at fixed subsystem rest densities the effective mass cannot drop below the asymptotic value reached for the completely separated ellipsoids. However, the effective mass for ground state matter, determined as a function of the increasing baryon vector density, decreases below this limit. This leads to an overprediction of the scalar attraction in CNM and a correspondingly smaller value of the attributed momentum k. The interplay between these two effects creates the differences in the mean field potential.

A correct determination of the effective mass, respectively the scalar density is an important issue, not only with respect to the nucleon potential. Also mesons like pions, kaons, ρ-mesons ect. are assumed to change their properties in a dense nuclear environment [38]. For the pseudo-scalar octet the Gell-Mann-Oakes-Renner relation [39] connects the vacuum mass with the expectation value of the scalar quark condensate. Within the framework of QCD inspired effective models, like NJL [40], effective chiral models [41] etc. the change of the scalar quark condensate in the medium is usually expressed in terms of the scalar baryon density. E.g. the resulting in-medium dispersion relation for kaons [42–44]

$$\omega_{\rm K^\pm}(\mathbf{k}) = \sqrt{\mathbf{k}^2 + m_{\rm K}^2 - \frac{\Sigma_{KN}}{f_\pi^2}\varrho_S + V_0^2} \pm V_0 \tag{51}$$

contains an attractive scalar part $\Sigma_{KN}/(f_\pi^2)\varrho_S$ and the vector potential $V_\mu = 3/(8f_\pi^2)j_\mu$ which is of different sign for kaons and antikaons. In particular kaons are primordially produced in the early and high density phase of the collisions [42] which means that they are born into an environment which resembles to large extent colliding matter. Already at SIS energies but particularly at AGS energies [45] the scalar density can be given by the asymptotic value (26) for the corresponding CNM configuration, characterized by high streaming velocities, large γ-factors and high ρ_B. Hence the LDA will lead to an overestimation of the scalar density and the corresponding mass reduction of these particles.

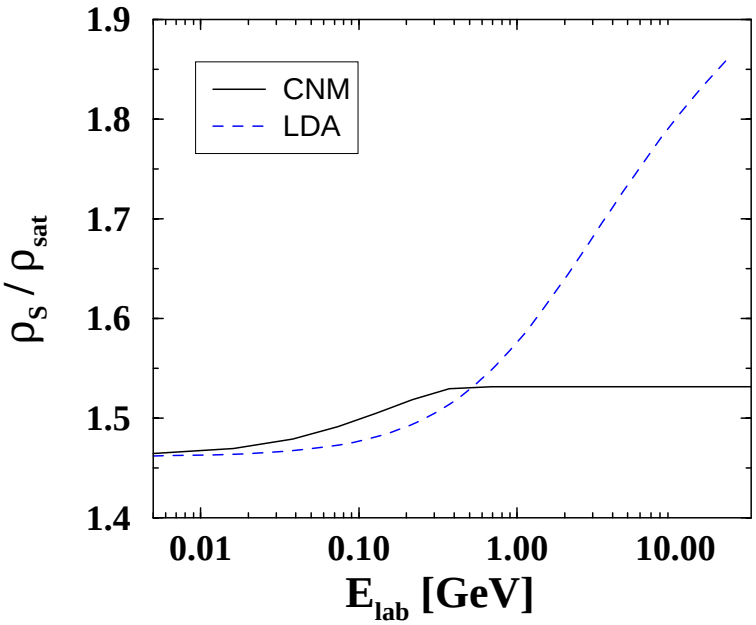

FIG. 12. Scalar density in colliding nuclear matter (CNM) at subsystem densities $\varrho_0 = \varrho_{\rm sat}$ as a function of the laboratory energy determined in the Walecka Model QHD-I. The result is compared to the corresponding effective mass in nuclear matter obtained in a local density approximation to the colliding system.

To estimate this effect in Fig.12 we show the scalar density in CNM as a function of the laboratory energy and compare to the LDA result. The laboratory energy of the asymptotically non-interacting system is given by $E_{\rm lab} = M(\gamma(v) - 1) = 2M(\gamma^2(u) - 1)$ where v is the laboratory velocity and u is again the c.m. streaming velocity. The subsystem rest densities are again chosen as $\varrho_0 = \varrho_{\rm sat}$ and QHD-I is used. The system is not compressed above $2\varrho_0$, i.e. the increase of $\rho_B = 2\gamma(u)\varrho_0$ is only due to the relative motion of the two currents. In the LDA the Lorentz contraction is interpreted as compression and the scalar density is calculated at the correspondingly enlarged Fermi momentum. Evidently this standard procedure yields completely different results.

Consequences for observables, in particular collective flow observables, have been discussed in [25]. The considered non-equilibrium effects reduce the transverse flow which is consistent with the softening of the effective EOS discussed in Sec. III. The magnitude

of this effect was found to be of the order as the usage of different (soft/hard) mean field parameterizations.

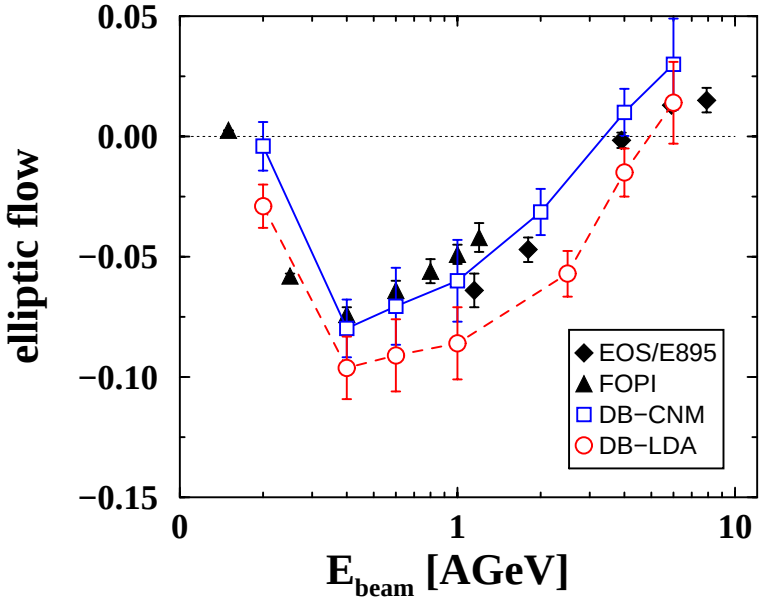

FIG. 13. Excitation function of the elliptic flow v_2 in $Au+Au$ reactions at mid-rapidity. The data are taken from the FOPI- (triangles) [46], and EOS/E895 (diamonds) [22] collaborations. RBUU calculations are performed with DB forces applied in the local density approximation (LDA) and determing the mean field locally in the colliding nuclear matter approximation (CNM).

As an example we show in Fig. 13 the excitation function of the elliptic flow v_2 for $Au + Au$ reactions at mid-rapidity. The mean field in the corresponding RBUU calculations [47] is based on the DB model discussed in Sec. III. In the one case the mean field is simply treated in the local density approximation (LDA), in the second case the potentials for CNM were used. Here the local parameters $\varrho_0^{T/P}(\mathbf{x}, t)$ and $v_{\rm rel}(\mathbf{x}, t)$ are determined from the actual phase space distribution $f(\mathbf{x}, \mathbf{k}, t)$. Details of the calculations can be found in [25] and [47]. The two different treatments which are based on identical nuclear forces yield significantly different results for the v_2. Since v_2 at mid-rapidity is in particular sensitive to the EOS at supra-normal densities [3,22,47] these effects are here most pronounced. Using the local density approximation one would exclude the underlying EOS from the comparison to data

as too stiff. The more consistent treatment of momentum space anisotropies leads to the discussed net softening of the effective EOS in the course of the reaction and restores the agreement with experimental data. Therefore non-equilibrium effects should be taken into account on the level of the effective in-medium interaction which means to determine the mean field used in transport calculations consistently for colliding nuclear matter.

V. NON-RELATIVISTIC APPROACHES

Since non-relativistic mean fields are also widely used in transport models it is worthwhile to shortly consider this case, in particular with respect to the structure of the single particle potential. For this purpose we choose a simple interaction which can serve as an illustrative example. The non-relativistic problem of two Galilei transformed Fermi spheres has e.g. been treated in [16]. Using a spin-isospin averaged Skyrme force of the type

$$V(\mathbf{k},\mathbf{q};\mathbf{k}',\mathbf{q}') = t_0 + \frac{t_1}{2}\left[(\mathbf{k}-\mathbf{q})^2 + (\mathbf{k}'-\mathbf{q}')^2\right] + t_2(\mathbf{k}-\mathbf{q})\cdot(\mathbf{k}'-\mathbf{q}') \tag{52}$$

the energy density in nuclear matter reads

$$\epsilon = \frac{\tau}{2M} + \pi = \frac{\tau}{2M} + \frac{1}{2}t_0\varrho^2 + (t_1+t_2)\varrho\tau \quad . \tag{53}$$

Three-body forces which give rise to a quadratic density dependence of the mean field have been neglected in the interaction (52). Thus we restrict the present discussion to the two-body level. The kinetic part of the energy density is given by

$$\tau = \frac{\kappa}{(2\pi)^3}\int d^3k\ \mathbf{k}^2\Theta(k,k_F) = \frac{2}{5\pi^2}k_F^5 \tag{54}$$

with $\kappa = 4$ in spin-isospin saturated matter. The local mean field and the effective Landau mass are given by

$$U_{\rm loc}(k_F) = \frac{\partial\epsilon}{\partial\varrho} \quad , \quad \frac{1}{2m^*} = \frac{\partial\epsilon}{\partial\tau} \tag{55}$$

which yields the single particle potential

$$U_{\rm s.p.}(k_F,\mathbf{k}) = U_{\rm loc}(k_F) + \mathbf{k}^2\left(\frac{1}{2m^*}-\frac{1}{2M}\right) = t_0\varrho + (t_1+t_2)\tau + \mathbf{k}^2(t_1+t_2)\varrho \quad . \tag{56}$$

The energy density in non-relativistic colliding matter, i.e. for two separated spheres ($Mu > 2k_F$) with subsystem densities $\varrho(k_F)$, total density $\varrho_{12}(k_{F_{tot}}) = 2\varrho(k_F)$ and c.m. streaming velocities $\pm u$ has the form [16]

$$\begin{aligned}
\epsilon_{12} &= \frac{\tau_{12}}{2M} + \pi_{12} \\
&= \frac{\kappa}{(2\pi)^3}\int \frac{d^3\mathbf{k}\ \mathbf{k}^2}{2M}\Theta_{12}(\mathbf{k}) + \frac{1}{2}\frac{\kappa^2}{(2\pi)^6}\int d^3\mathbf{k}\ d^3\mathbf{q} V(\mathbf{k},\mathbf{q};\mathbf{k},\mathbf{q})\Theta_{12}(\mathbf{k})\Theta_{12}(\mathbf{q}) \\
&= 2\frac{\tau(k_F)}{2M} + \varrho_{12}\frac{Mu^2}{2} + \frac{1}{2}t_0\varrho_{12}^2 + (t_1+t_2)\left[\varrho_{12}2\tau(k_F) + (\varrho_{12}Mu)^2\right] \\
&= \epsilon|_{2\kappa} + u^2\left[\varrho_{12}\frac{M}{2} + \varrho_{12}^2M^2(t_1+t_2)\right] \quad .
\end{aligned} \tag{57}$$

The different contributions in Eq.(57) are easy to interpret: Like in the relativistic case the energy density can be decomposed into a static part $\epsilon|_{2\kappa}$ which is determined by the doubled phase space volume, and a velocity dependent part. The latter contains the kinetic energy of the relative motion and the potential energy which originates from the integration of the interaction over the momentum spread of the two spheres, i.e. the interaction between the two currents. With (55) one obtains the local part of the single particle potential as

$$U_{\rm loc\ 12} = \frac{\partial\epsilon_{12}}{\partial\varrho_{12}} = U_{\rm loc\ 12}(k_F) + U'_{\rm loc\ 12}(k_F,u) \quad . \tag{58}$$

¿From (57) and (58) one finds that the velocity independent part of $U_{\rm loc}$

$$U_{\rm loc\ 12}(k_F) = \frac{\partial\epsilon|_{2\kappa}}{\partial\varrho_{12}} = 2U_{\rm loc}(k_F) \tag{59}$$

equals two times the potential in nuclear matter at half the total density, i.e. it behaves like the scalar part of the relativistic mean field. In both cases the differences between the local potentials derived in NM and CNM originate from non-linear density dependence, (55), respectively the momentum integration over the interaction which creates this density dependence. In the relativistic case the M^*/E^* weights (21,26) play this role. Thus the reduced Fermi pressure affects not only the kinetic but also the internal potential energy of

the subsystems. Although the Skyrme force (52) will lead to unrealistic quantitative predictions for CNM at large velocities (it was especially designed for small relative momenta) it serves as an instructive example for a momentum dependent two-body interaction. The same qualitative arguments are valid when a more realistic interaction, e.g. the Brueckner G-matrix, is used in (57). A stronger binding in colliding nuclear matter has e.g. been observed in non-relativistic G-matrix calculations for colliding matter [14], but without giving an interpretation.

One should be aware that this type of phase space effects is not included in standard transport calculations for heavy ion collisions, even when momentum dependent interactions are used. Phenomenological potentials are usually composed by a local, density dependent potential and a non-local momentum dependent part [21]. For a nucleon with momentum $\mathbf{k}$ the single particle potential derived from the phase space distribution $f(\mathbf{q}) \propto \Theta_{12}(\mathbf{q})$ reads

$$\begin{aligned} U_{\text{s.p.}}(k_{F_{\text{tot}}}, \mathbf{k}) &= U_{\text{loc}}(k_{F_{\text{tot}}}) + \frac{4}{(2\pi)^3} \int d^3q \; V(\mathbf{k}, \mathbf{q}; k_{F_{\text{tot}}}) \Theta_{12}(\mathbf{q}) \\ &= U_{\text{loc}}(k_{F_{\text{tot}}}) + U_{\text{nonloc}}(k_{F_{\text{tot}}}, \mathbf{k}) \quad . \end{aligned} \tag{60}$$

In transport calculations U_{nonloc} arises from the integration of an effective two-body interaction over the actual momentum distribution f. Thus U_{nonloc} accounts properly for the spread in momentum space between projectile and target nucleons as well as for the reduced Fermi momenta inside the subsystems. The same procedure should be applied to the local part of the potential. However, in standard transport calculations the density dependence of the mean field is parameterized into U_{loc} as a function of the total density. This density dependence is decoupled from the momentum space anisotropy and differs from (58). Consequently, $U_{\text{loc}}(k_{F_{\text{tot}}})$ reflects the density dependence of equilibrated matter but should be calculated consistently also for anisotropic momentum space configurations.

VI. SUMMARY

The early as well as high density phase of relativistic heavy ion reactions from SIS up to AGS energies are to large extent governed by phase space configurations far from local

equilibrium. The phase space of the participant matter can be approximated by counter-streaming or colliding nuclear matter. In the present work we discussed implications for the nuclear equation of state which occurs in such non-equilibrium configurations. We restricted the discussion to the temperature zero case.

The EOS in colliding matter is determined by two competing effects: The separation of phase space reduces the Fermi pressure in the subsystems compared to ground state matter. The reduction of the internal subsystem Fermi momenta affects also the potential part of the energy density and leads to an enlarged binding energy in the total system. For scalar quantities, e.g. the effective mass, the separation of phase space has is (in mean field approximation) formaly equivalent to the introduction of an additional degree of freedom. Using a more realistic interaction derived from the in-medium Dirac-Brueckner T-matrix this effect is present as well, but modified by the superimposed explicit momentum dependence of the interaction. Due to the repulsive character of the nuclear forces at high momenta, the relative motion of the two currents leads, on the other hand, to a strong additional repulsion in the system. The latter effect originates from the interaction between projectile and target nucleons and is taken into account by transport calculation when momentum dependent forces are used. The modification of the internal mean field of the subsystems by the separation in phase space is, however, not included in standard transport calculations. The magnitude of the discussed non-equilibrium effects is model dependent, however, the qualitative picture is model independent.

In order to discuss the consequences for the equation of state in non-equilibrium, an effective EOS for colliding matter has been constructed where the energy of the relative motion has been subtracted. It was found as a model independent feature, that the separation of phase space leads to a considerable softening of the EOS in colliding matter. This effect is present over a wide range of densities and streaming velocities. We conclude that the discussed non-equilibrium effects should be taken into account when transport calculations for heavy ion collisions are performed.

ACKNOWLEDGMENTS

We would like to thank H.H. Wolter for many discussions.

---

[1] H. Stöcker and W. Greiner, Phys. Rep. **137**, 277 (1986).

[2] W. Reisdorf and H.G. Ritter, Annu. Rev. Nucl. Part. Sci. **47**, 663 (1997);
N. Herrmann, J.P. Wessels, T. Wienold, Annu. Rev. Nucl. Part. Sci. **49**, 581 (1999).

[3] P. Danielewicz, Roy A. Lacey, et al., Phys. Rev. Lett. **81**, 2438 (1998);
C. Pinkenburg *et al.*, Phys. Rev. Lett. **83**, 1295 (1999).

[4] J. Aichelin and C.M. Ko, Phys. Rev. Lett. **55**, 2661 (1985).

[5] C. Sturm *et al.* (KaoS Collaboration), Phys. Rev. Lett. **86**, 39 (2001).

[6] C. Fuchs, Amand Faessler, E. Zabrodin, Y.-M. Zheng, Phys. Rev. Lett. **86**, 1974 (2001).

[7] F. Rami et al. (FOPI Collaboration), Phys. Rev. Lett. **84**, 1120 (2000).

[8] L. Sehn, H.H. Wolter, Nucl. Phys. **A601**, 473 (1996);
C. Fuchs, L. Sehn, H.H. Wolter, Nucl. Phys. **A601**, 505 (1996).

[9] B. Blättel, V. Koch, W. Cassing, U. Mosel, Phys. Rev. C **38**, 1767 (1988).

[10] J. Aichelin, Phys. Rep. **202**, 233 (1991).

[11] C. Fuchs, P. Essler, T. Gaitanos, H. H. Wolter, Nucl. Phys. **A626**, 987 (1997).

[12] A. Lang, B. Blättel, W. Cassing, V. Koch, U. Mosel and K. Weber, Z. Phys. **A340** (1991) 287.

[13] R.K. Puri, N. Ohtsuka, E. Lehmann, A. Faessler, M.A. Matin, D.T. Khoa, G. Batko, S.W. Huang, Nucl. Phys. **A575** (1994) 733.

[14] N. Ohtsuka, R. Linden, A. Faessler, F.B. Malik, Nucl. Phys. **A465**, 550 (1987).

[15] K. Weber, B. Blättel, W. Cassing, H.C. Dönges, A. Lang, T. Maruyama, and U. Mosel, Nucl. Phys. **A552**, 571 (1993).

[16] L.W. Neise, H. Stöcker, W. Greiner, J. Phys. G **13** L181 (1987).

[17] Y.B. Ivanov, V.N. Russkihk, M. Schönhofen, M. Cubero, B.L. Friman, W. Nörenberg, Z. Phys. **A340**, 385 (1991).

[18] H, Elsenhans, L. Sehn, A. Faessler, H. Müther, N. Ohtzuka, H.H. Wolter, Nucl. Phys. **A536**, 750 (1992).

[19] L.W. Neise, thesis, Frankfurt (1990), GSI report GSI-90-24.

[20] L. Sehn, thesis (1990) unpublished.

[21] G.M. Welke *et al.*, Phys. Rev. C **38**, 2101 (1988); C. Gale *et al.*, Phys. Rev. C **41**, 1545 (1990).

[22] P. Danielewicz, Nucl. Phys. **A673**, 275 (2000).

[23] W. Botermans, R. Malfliet, Phys. Rep. **198**, 115 (1990).

[24] I. Izumoto, S. Krewald, A. Faessler, Nucl. Phys. **A341**, 319 (1980).

[25] C. Fuchs, T. Gaitanos, H. H. Wolter, Phys. Lett. B **381**, 23(1996);
T. Gaitanos, C. Fuchs, H. H. Wolter, Nucl. Phys. **A650**, 97 (1999).

[26] B. D. Serot, J. D. Walecka, Advances in Nuclear Physics, **16**, 1, eds. J. W. Negele, E. Vogt, (Plenum, N.Y., 1986).

[27] J. Boguta, Phys. Lett. B **109**, 251 (1982).

[28] B. ter Haar, R. Malfliet, Phys. Rep. **149**, 207 (1987).

[29] T. Gross-Boelting, C. Fuchs, and A. Faessler, Nucl. Phys. **A648**, 105 (1999).

[30] P. Dupieux *et al.*, Nucl. Phys. **A587**, 802 (1995).

[31] C.J. Horowitz and B.D. Serot, Nucl. Phys. **A464**, 613 (1987).

[32] J.A. Tjon and S.J. Wallace, Phys. Rev. C **32**, 1667 (1985).

[33] C. Fuchs, H. Lenske, H. H. Wolter, Phys. Rev. C **52**, 3043 (1995);
H. Lenske and C. Fuchs, Phys. Lett. B **345**, 355 (1995).

[34] R.J. Furnstahl, B.D. Serot, and H.-B. Tang, Nucl. Phys. **A615**, 441 (1997);
H.W. Hammer, R.J. Furnstahl, Nucl. Phys. **A678**, 272 (2000).

[35] E.D. Cooper *et al.*, Phys. Rev. C **36**, 2170 (1987).

[36] C. Fuchs, E. Lehmann, L. Sehn, F. Scholz, J. Zipprich, T. Kubo, and Amand Faessler, Nucl. Phys. **A603**, 471 (1996).

[37] B.M. Waldhauser, M. Maruhn, H. Stöcker, W. Greiner, Phys. Rev. C **38**, 1003 (1988).

[38] G.E. Brown and M. Rho, Phys. Rep. **269**, 333 (1996).

[39] M. Gell-Mann, R. Oakes, B. Renner, Phys. Rev. **175**, 2195 (1968).

[40] S. Klimt, M. Lutz, W. Weise, Phys. Lett. B **249**, 386 (1990);
T. Maruyama, K. Tsushima and A. Faessler, Nucl. Phys. **A535**, 497 (1991); *ibid* Nucl. Phys. **A537**, 303 (1992).

[41] B. D. Kaplan and A. E. Nelson, Phys. Lett. B **175**, 57 (1986);
A. E. Nelson and B. D. Kaplan, Phys. Lett. B **192**, 193 (1987).

[42] G.Q. Li, C.M. Ko and B.A. Li, Phys. Rev. Lett. **74**, 235 (1995);
G.Q. Li, C.M. Ko, Nucl. Phys. **A594**, 460 (1995).

[43] J. Schaffner, J. Bondorf, I. N. Mishustin, Nucl. Phys. **A625**, 325 (1997).

[44] C. Fuchs, D. Kosov, Amand Faessler, Z.S. Wang and T. Waindzoch, Phys. Lett. B **434**, 254 (1998).

[45] Subrata Pal, C.M. Ko, Ziwei Lin, Bin Zhang, Phys. Rev. C **62**, 061903 (2000).

[46] A. Andronic *et al.* (FOPI collaboration), Nucl. Phys. **A661**, 333c (1999).

[47] T. Gaitanos, C. Fuchs, H. H. Wolter, A. Faessler, Eur. Phys. J. **A12**, 421 (2001).